

Interfacial Engineering of a Heteroatom-Doped Graphene Layer on Patterned Aluminum Foil for Ultrafast Lithium Storage Kinetics

Dong-Yo Shin and Hyo-Jin Ahn*

Cite This: *ACS Appl. Mater. Interfaces* 2020, 12, 19210–19217

Read Online

ACCESS |



Metrics & More



Article Recommendations

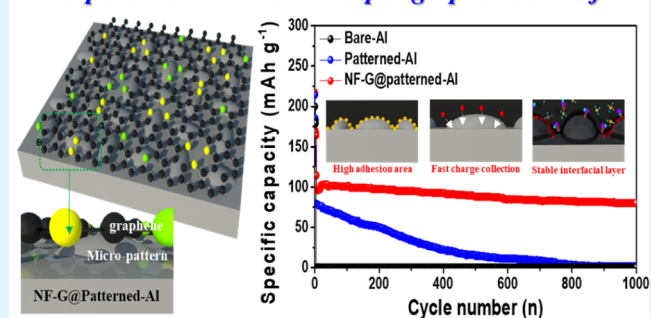


Supporting Information

ABSTRACT: The design of the interfacial architecture between the electrode and the current collector in lithium-ion batteries (LIB) plays a key role in achieving ultrafast lithium storage kinetics with respect to efficient charge transfer and cycle stability. However, in recent years, despite considerable efforts in the structural and chemical engineering of active materials (anode and cathode materials), interfacial architectures between the electrode and the current collector have received relatively insufficient attention in the case of ultrafast LIBs. Here, the interface architecture of a micropatterned Al current collector with a heteroatom-doped graphene interfacial layer is developed using roll pressing and dip coating processes. The cathode electrode fabricated with the resultant current collector offers increased contact area with enhanced interfacial stability between the electrode and the current collector because of micropatterns with heteroatom-doped graphene formed on the current collector, leading to outstanding ultrafast cycling capacity ($105.8 \text{ mA h g}^{-1}$) at 20 C. Furthermore, at extremely high rate and long-term cycling performance, significant ultrafast cycling stability (specific capacity of 87.1 mA h g^{-1} with capacity retention of 82.3% at 20 C after 1000 cycles) is noted. These improved ultrafast and ultra-stable performances are explained in terms of the increased electron collection/provision site with a high contact area between the electrode and the current collector for enhanced ultrafast cycling capacity and the effective corrosion prevention of the current collector with fast charge transfer for ultrafast cycling stability.

KEYWORDS: lithium ion batteries, ultrafast, current collector, interface architecture, micro-patterns

Micro-patterns with N and F doped graphene on Al foil



INTRODUCTION

In recent years, oil shortage has emerged as a global issue with many attempts to replace gasoline-powered devices with electrically powered devices such as electric vehicles, unmanned drones, and electric trains.^{1–3} However, these electrically powered devices are still limited in their practical applications because of critical problems such as long charging times, low mileage per charge, and short life times.^{4–7} To overcome this problem, the reduction of body weight, improvement of motor efficiency, and reduced charging times have become important issues. Lithium-ion batteries (LIB) have high energy densities, have long life times, are eco-friendly, and exhibit low self-discharge. Because of these characteristics, they have great potential to serve as the main power source for high-technology electrical devices.^{8,9} However, despite the aforementioned advantages, LIBs still suffer from low ultrafast cycling performances with poor life times which prevents their widespread application in high-technology electrical devices. To reduce the charging time of electric vehicles, battery manufacturers are developing new electrode materials, electrolytes, and additives. Some companies are targeting electric vehicles that can be fully charged

within 6 min (C-rate of >10 C). This is problematic as it causes the battery lifetime to drastically decline, with some batteries even exploding. As a possible solution to these problems, interfacial engineering has shown great potential as a key technology that offers enhanced electrical, mechanical, chemical, and electrochemical properties by using geometric architectures and unique structural designs.^{10–12} In particular, in recent years, as corrosion and exfoliation problems of the interface between the electrode and the current collector have emerged, a strategy of interface coating such as metal oxide and carbon material to enhance the ultrafast cycling stability has been developed at the current collector.^{13–16} For example, Ma et al. conducted a study on corrosion of the Al foil as the current collector occurring during the electrochemical reaction in LIBs.¹³ They suggested that corrosion of the current

Received: February 3, 2020

Accepted: April 1, 2020

Published: April 1, 2020



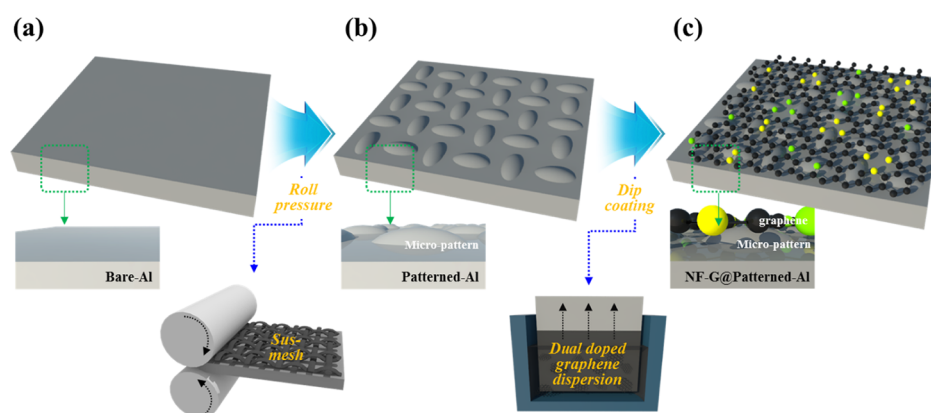


Figure 1. Schematic illustration of process steps of (a) bare-Al, (b) micropatterned Al foil, and (c) NF-G@micropatterned Al foil to fabricate the N and F doped graphene interfacial layer on micropatterned Al foil.

collector should be suppressed to increase the cycling stability of LIBs. Furthermore, Wang et al. fabricated graphene-coated Al foil as the current collector in LIBs using plasma-enhanced chemical vapor deposition.¹⁴ The electrode fabricated by graphene-coated Al foil showed the increased cycling stability ($\sim 92 \text{ mA h g}^{-1}$ with capacity retention of 91% after 360 cycles at 0.5 C) with high rate capacity ($\sim 60 \text{ mA h g}^{-1}$ at 5 C). The authors proposed that the introduced graphene coating layer can effectively prevent the attack of the current collector by electrolyte decomposition. However, critical problems, in which ultrafast cycling performances are extremely decreased, newly occurred because of the low electrical conductivity of the coating layer. Therefore, novel strategy of interfacial engineering which can support the ultrafast cycling capacity with ultra-stable cycling performance is needed to solve the main problems of the existing ultrafast LIBs.

In this study, we design a novel interface architecture of a heteroatom (N and F)-doped graphene interfacial layer on micropatterned Al foil as a current collector of the cathode electrode for accelerating the lithium storage kinetics and interfacial stability of LIBs. The micropatterns and graphene interfacial layer were formed on Al foil by roll pressing and dip coating processes. Specially, this technique provides an improved lithium storage kinetics and greatly improves interfacial stability. This novel interface engineering dramatically improves the ultrafast and ultra-stable cycling performance even at 20 C when it was introduced at the cathode fabricated with a current collector in LIBs.

RESULTS AND DISCUSSION

Figure 1 shows a schematic illustration of the micropatterning and graphene coating processes on Al foil. The micropatterned Al foil is formed by physical pressing using a conventional roll press with a SUS mesh having a wire diameter of $\sim 50.8\text{--}56.2 \mu\text{m}$ with a pore size of $\sim 113.7\text{--}138.4 \mu\text{m}$ (Figure S1). The distance between the patterns and micropattern size is determined by the mesh type and compressive force (Figures S2 and S3). In addition, micropatterns having ellipsoid morphology appear because of the structure of the mesh pattern. The formed micropatterns on Al foil are important in enhancing the adhesion by improving the contact area between the electrode and the current collector. The graphene interfacial layer on patterned Al foil is formed by a dip coating process with suspension containing the N- and F-doped graphene (Figure S4). The N- and F-doped graphene

interfacial layer has excellent electrical conductivity and superb electrochemical properties because of its unique crystal structure resulting from C–N and C–F bonds.¹⁷ The N- and F-doped graphene is formed by thermal decomposition and bonding reaction of ammonium fluoride (NH_4F) which acts as the N and F doping sources. The thermal decomposition equation of NH_4F is as follows.¹⁸



Initially, NH_4F is thermal-decomposed to ammonia (NH_3) and hydrogen fluoride (HF) at $>100 \text{ }^\circ\text{C}$. Then, as the temperature increases, the decomposition products NH_3 and HF act as doping sources of N and F during the calcination process at more than $300 \text{ }^\circ\text{C}$ (Figures S5 and S6).^{17,18} The prepared N- and F-doped graphene powders are then dispersed in NMP as suspension for the dip coating process. The N- and F-doped graphene in suspension is uniformly coated on the micropatterned Al foil. Introduction of the N- and F-doped graphene interfacial layer on micropatterned Al foil can be an effective strategy to prevent the corrosion of Al foil and quickly electron transfer at the interface between the electrode and Al foil during ultrafast cycling.

Figure 2 shows the top-view field emission scanning electron microscopy (FESEM) images of bare-Al, patterned-Al, and

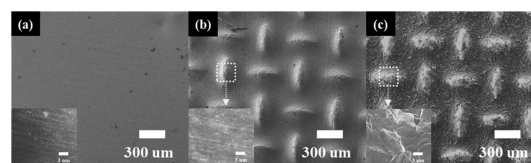


Figure 2. Top-view FESEM images of (a) bare-Al, (b) patterned-Al, and (c) NF-G@patterned-Al.

NF-G@patterned-Al. The bare-Al (Figure 2a) showed a smooth surface without any shape while the patterned-Al surface (Figure 2b) exhibited a micro-pattern morphology which consists of an ellipse shape with a diameter of $\sim 326.1\text{--}346.8 \mu\text{m}$ (aspect ratio of 3.10). The NF-G@patterned-Al exhibits a rough surface because of the N- and F-doped graphene interfacial layer being coated with micropatterns with a diameter of $\sim 326.8\text{--}348.8 \mu\text{m}$ (aspect ratio of 3.09) (see Figure 2c) and a thickness of $0.48\text{--}0.61 \mu\text{m}$ after the dip coating process (see Figure S7).^{19,20} In the case of NF-G@patterned-Al, the N- and F-doped graphene interfacial layer is

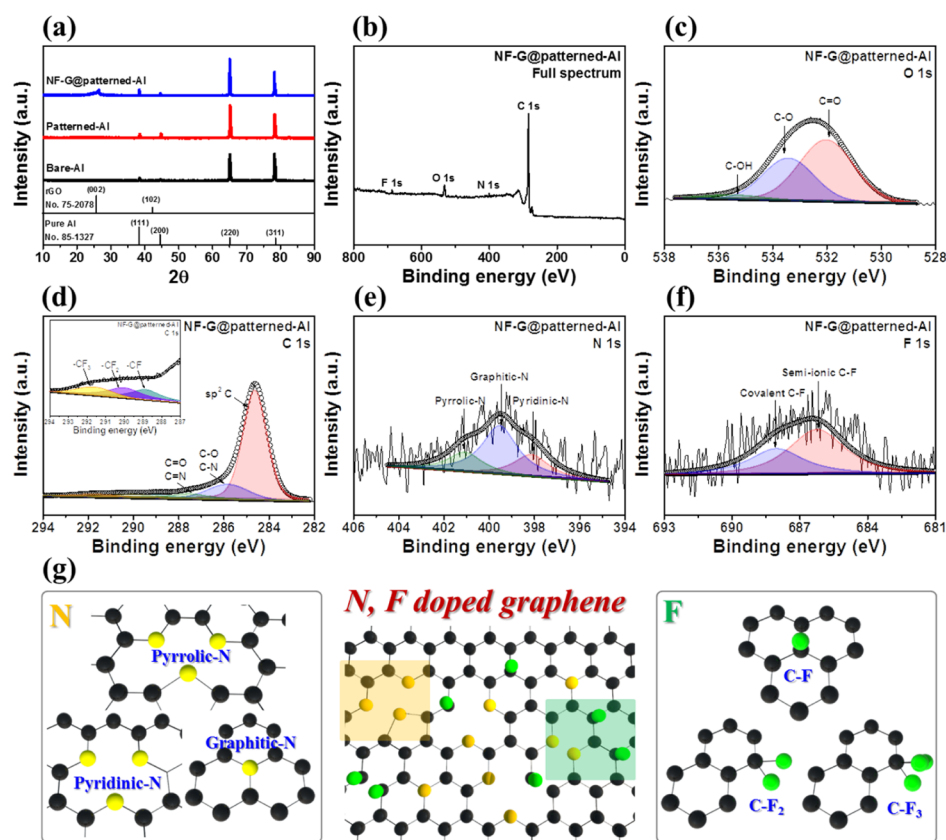


Figure 3. (a) XRD data of all samples, (b) XPS full scan spectrum of NF-G@patterned-Al, XPS spectra obtained from (c) O 1s, (d) C 1s, (e) N 1s, (f) F 1s, and (g) schematic illustration of N and F doped graphene.

uniformly formed at both the top and bottom area (see the inset of Figure 2c). This layer acts as a conductive passivation layer that can increase ultrafast cycling performance by preventing Al foil corrosion while also offering a charge transfer pathway.^{21,22} In addition, in the laser scanning microscopy (LSM) images, the heights of the micropattern in patterned-Al and NF-G@patterned-Al were ~ 42.3 and ~ 43.4 μm , respectively (Figure S8).

Figure 3a displays the X-ray diffraction (XRD) patterns of bare-Al, patterned-Al, and NF-G@patterned-Al. The main characteristic diffraction peaks of all samples were exhibited at ~ 38.5 , ~ 44.7 , ~ 65.1 , and $\sim 78.2^\circ$, corresponding to (111), (200), (220), and (311) planes of Al phases, which match with the space group of $Fm\bar{3}m$ (JCPDS card no. 85-1327).²² The bare-Al and patterned-Al only exhibited diffraction peaks of Al without any other phases. The diffraction peaks of the NF-G@patterned-Al, along with the peaks related to Al, are observed at ~ 26.7 and $\sim 43.5^\circ$, corresponding to (002) and (101) planes of reduced graphene oxide phase with the space group of $p\bar{3}1m$ (JCPDS card no. 75-2078) because of the N- and F-doped graphene interfacial layer coated on Al foil.^{23,24} To demonstrate the chemical states of the NF-G@patterned-Al, X-ray photoelectron spectroscopy (XPS) analysis was performed, as shown in Figure 3b–g. Figure 3b shows the XPS full scan spectrum of NF-G@patterned-Al to confirm the presence of O, C, N, and F without other elements. The O 1s spectrum of NF-G@patterned-Al (Figure 3c) displayed at ~ 532.0 , ~ 533.4 , and ~ 535.4 eV corresponds to different bonding states of C=O, C–O, and C–OH.²⁵ The C–O bonding state is formed by the N- and F-doped graphene interfacial layer on the patterned-Al foil. The C 1s XPS

spectrum of NF-G@patterned-Al (Figure 3d) indicated six signals at ~ 284.6 , ~ 285.9 , ~ 287.5 , ~ 289.9 , ~ 291.6 , and ~ 293.3 eV, corresponding to the sp^2 C, C–O/C–N, C=O/C=N, C–F, C–F₂, and C–F₃ bonds.^{25,26} In general, sp^2 C constituting the graphene layer is composed of one s-orbital and two p-orbitals. These are each bonded at 120° to form C–C bonds, which is a honeycomb structure.²⁷ It is well known that the honeycomb structure of graphene has high electrical conductivity by forming electron clouds because of the presence of π -electrons, which occurs by sp^2 C bonds.²⁷ The N 1s spectrum of NF-G@patterned-Al showed three signals at ~ 398.2 , ~ 399.5 , and ~ 401.0 eV, corresponding to the pyridinic-, graphitic- (or quaternary-), and pyrrolic-N bonds (Figure 3e).²⁸ The pyridinic-N bonding is located at the edge sites of the graphene basal plane combined with two C atoms. The pyrrolic-N bonding forms heterocyclic rings which are bonded to two C atoms at the graphene basal plane. The pyridinic-N and pyrrolic-N are well known for providing two p electrons by π systems of carbon.²⁸ The graphitic-N is formed by N atoms substituting C atoms in C–C bonding. The N–C bonding can increase the electrical properties because the electronegativity of N atoms (3.04) is higher than C atoms (2.55).²⁷ The F 1s binding energies of NF-G@patterned-Al are located at ~ 686.2 and ~ 688.1 eV, corresponding to semi-ionic C–F and covalent C–F (Figure 3f).²⁹ These bonds are formed by the interaction of sp^2 and sp^3 hybridization carbon atoms in graphene. Furthermore, the C–F bonds are well formed at defects in graphene such as the edge plane, O-containing functional groups, and N-containing functional groups because of the strong electronegativity of the F atom (3.98).²⁹ The C–F bonding can improve charge transfer and accessibility by

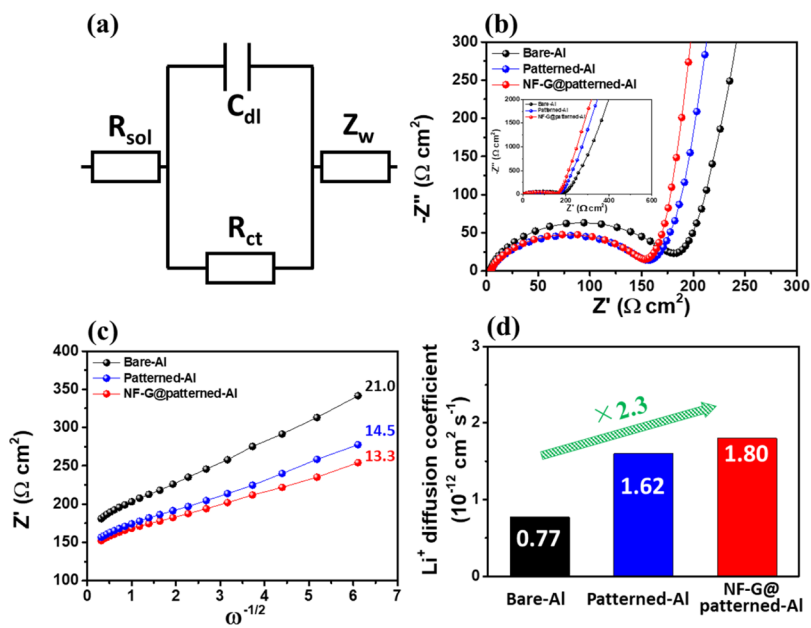


Figure 4. (a) Equivalent circuit used EIS analysis, (b) Nyquist plots of all electrodes, (c) relationship between Z_{real} and $\omega^{-1/2}$ in the low frequency range of all electrodes, and (d) Li^+ ion diffusion coefficient of all electrodes.

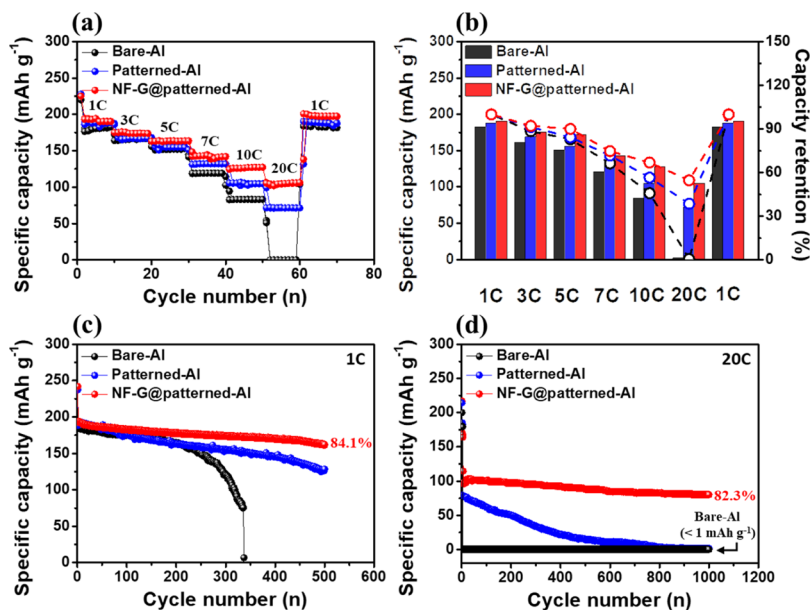


Figure 5. (a) Rate-performance at a current density of 1, 3, 5, 7, 10, 20, and 1 C, (b) specific capacity and capacity retentions of bare-Al, patterned-Al, NF-G@patterned-Al electrodes with increasing current densities, (c) cycling test at a current density of 1 C during 500 cycles, and (d) long-term cycling test at 20 C up to 1000 cycles.

extending ion diffusion space and decreasing the charge absorption/desorption energy barrier. Therefore, the doped N and F atoms in graphene improves the electrical conductivity, charge accessibility, and ion diffusion rate of the graphene, thereby improving the electrical/electrochemical properties (Figures 3g and S9). In addition, the defect structure of N- and F-doped graphene is investigated by Raman spectroscopy, as shown in Figure S10. The I_D/I_G ratio (1.04) of N- and F-doped graphene, which indicates the defect structure of graphene, is higher than the I_D/I_G ratio (0.92) of graphene because of increased defects in the graphene lattice by doped N and F atoms.^{30,31} Thus, the XRD, XPS, and Raman results

demonstrate that the N- and F-doped graphene interfacial layer was well formed on the NF-G@patterned-Al foil surface.

To investigate the electrochemical kinetics corresponding to charge transfer resistance and Li^+ ion diffusion in fresh cells fabricated with bare-Al, patterned-Al, and NF-G@patterned-Al, the corresponding electrochemical impedance spectroscopy (EIS) was analyzed. Figure 4b exhibits the Nyquist plots of all electrodes at open-circuit potential at frequencies from 10^5 kHz to 10^{-2} Hz. The EIS data appear in two parts of the semicircle and the inclined line at the low frequency region and the high frequency region. The semicircle consisting of double-layer capacitance (C_{dl}) and charge transfer resistance (R_{ct}) is attributed to absorption of charges on the electrode interface

and the redox reaction on the electrode, respectively (Figure 4a).^{32,33} The inclined line corresponds to the Warburg impedance which is Li ion diffusion in the electrode.^{32,33} In Figure 4b, the bare-Al electrode shows a high semicircle with high Warburg impedance, which signifies poor charge transfer kinetics because of limited electron providing/collecting sites by a low contact area between the electrode and the current collector. On the other hand, the semicircle of the patterned-Al and NF-G@patterned-Al electrodes indicates a lower than bare-Al electrode. In general, the size of the semicircle in EIS data mainly depends on charge transfer resistance, and the patterned-Al and the NF-G@patterned-Al electrodes have a low charge transfer resistance because of the improved electron collection/provision site between the electrode and the current collector (Figure S11).^{34,35} In particular, the NF-G@patterned-Al electrode indicates the lowest Warburg impedance and the lowest charge transfer resistance among the samples (Figure 4c). This result is due to the formation of micropatterns with N- and F-doped graphene interfacial layer that can increase the electron collection/provision site and fast electron transfer on the current collector interface. In addition, the diffusion coefficient of the Li ion (Figure 4d) can be calculated from the inclined line in the low-frequency region by the following equation.^{12,36}

$$Z_{\text{real}} = R_e + R_{\text{ct}} + \sigma_w \omega^{-1/2} \quad (2)$$

$$D = R^2 T^2 / 2A^2 n^4 F^4 C^2 \sigma_w^2 \quad (3)$$

where, R_e is bulk resistance in the cell related to overall resistance of an electrode, a separator, and an electrolyte. R_{ct} is the charge transfer resistance between the electrode and electrolyte. σ_w is the Warburg impedance coefficient. R , T , and A denote the gas constant, operating temperature, and electrode area, respectively. n , F , and C signify the number of electrons per molecule, Faraday constant, and molar concentration of Li ion, respectively. The diffusion coefficients of Li ion for bare-Al, patterned-Al, and NF-G@patterned-Al electrode are 0.77×10^{-12} , 1.62×10^{-12} , and 1.80×10^{-12} $\text{cm}^2 \text{s}^{-1}$, which is calculated by σ_w respectively. This result indicates that micropatterns with N- and F-doped graphene interfacial layer could efficiently improve the ionic diffusion rate during an ultrafast charge–discharge process. Thus, low charge transfer resistance with superior Li ion diffusion coefficient of NF-G@patterned-Al can increase the ultrafast Li storage performance because of the enhancement of electron transfer and Li ion diffusion kinetics.

Figure 5a displays the rate performance of all electrodes at various C-rates of 1, 3, 5, 7, 10, and 20 C. With an increase of the C-rate, the specific capacity of the bare-Al electrode is completely degraded at a current density of 20 C. In contrast, even at a high rate of 20 C, the specific capacities of the patterned-Al and NF-G@patterned-Al electrode are 71.8 and 105.8 mA h g^{-1} , respectively. This result indicates a superb ultrafast cycling performance compared to previous reports of cathode electrode constructed with the NCA material. Especially, at 20 C, compared to 1 C, although the capacity retention of bare-Al is under 1%, capacity retentions of patterned-Al and NF-G@patterned-Al electrodes are 38.6 and 54.7%, respectively (Figure 5b). In addition, the coulombic efficiency of the NF-G@patterned-Al electrode (>99.2%) is higher than the bare-Al electrode (>98.8%) at all current densities (Figure S12). This is mainly attributed to the facilitated electron and Li ion diffusion on the Al foil by the

introduction of the micropatterns and the N- and F-doped graphene interfacial layer.^{12,33} Specifically, the NF-G@patterned-Al exhibits excellent specific capacity of 168.8 mA h g^{-1} with a capacity retention of 84.1% at a current density of 1 C after 500 cycles, which is attributed to the increased adhesion area between the electrode and the current collector resulting from micropatterns with the N- and F-doped graphene interfacial layer (Figure 5c). The cathode fabricated with bare-Al foil as the current collector performs well at a current density of 1 C, and the ultrafast charge/discharge performance at 20 C may rapidly decrease because of severe electrode exfoliation by volume expansion of the cathode material.^{11,33} The charge/discharge performance may also be affected by poor electrochemical kinetics because of the limited electron transfer rate and Li ion diffusion. In order to demonstrate the effect of the N- and F-doped graphene interfacial layer on micropatterned Al foil, we measured the ultrafast cycling test of all electrodes at a high current density of 20 C during 1000 cycles. As shown in Figure 5d, while the bare-Al electrode exhibits an extremely low specific capacity under 1 mA h g^{-1} during the 1000 cycles at a current density of 20 C, the NF-G@patterned-Al electrode exhibits a noticeable enhancement of the ultrafast cycling performances with high specific capacity (87.1 mA h g^{-1}) and superb capacity retention (82.3%). After the cycling test of 1000 cycles at 20 C, the cell was disassembled and the bare-Al electrode was found to have suffered from electrode decomposition and peeling phenomenon, which is attributed to severe degradation by low interfacial stability.

Figure 6 exhibits the surface morphology of the bare-Al and NF-G@patterned-Al electrode after 1000 cycles at 20 C. The

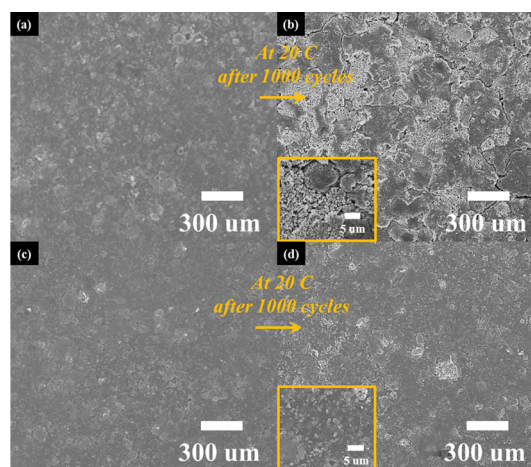


Figure 6. FESEM images of (a,c) initial and (b,d) after ultrafast cycling performance during 1000 cycles at 20 C obtained from electrodes fabricated by bare-Al and NF-G@patterned-Al, respectively.

bare-Al and NF-G@patterned-Al electrode display the smooth surface morphology without surface cracks and breakage (Figure 6a,c). After 1000 cycles under ultrafast cycling condition (20 C), however, the bare-Al electrode was severely damaged with surface crack and breakage because of electrode decomposition by electrode exfoliation and corrosion of the current collector (Figure 6b). On the other hand, the NF-G@patterned-Al showed a surface structure similar to the initial surface structure even after ultrafast cycling performance (Figure 6d) because of increased adhesion and corrosion

resistance by the micropatterned substrate and the N- and F-doped graphene interfacial layer. In addition, Figure S13 shows images of components in decomposed cells of bare-Al and NF-G@patterned-Al electrodes cycled at 20 C after 1000 cycles. The bare-Al electrode obtained from the measured cell during 1000 cycles at 20 C appeared broken surface and a separated electrode material. The NF-G@patterned-Al electrode exhibited relatively stable surface morphology when compared to the bare-Al electrode. This result suggests that the N- and F-doped graphene interfacial layer on micropatterned Al foil dramatically prevents the electrode exfoliation and corrosion of the current collector. Furthermore, in the case of EDS results after 1000 cycles at 20 C, while the Al components on surface of bare-Al electrode rapidly increased from 0.8 to 1.8 at. %, the Al components of NF-G@patterned-Al increased slightly from 0.8 to 1.1 at. % (Figure S14 and Table S2).

Figure 7 shows Nyquist plots of all electrodes obtained from cell of initial and after 1000 cycles at ultrafast cycling (20 C).

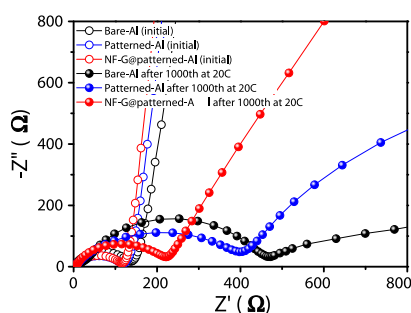


Figure 7. Nyquist plots of all sample electrodes obtained from initial and after 1000 cycles at a current density of 20 C.

The bare-Al and patterned-Al electrodes showed severely increased resistance with high Warburg impedance because of electrode breakage and exfoliation. However, despite the ultrafast cycling test at 20 C for 1000 cycles, because of improved adhesion area and enhanced corrosion resistance of the current collector, the NF-G@patterned-Al electrode with low resistance and low Warburg impedance was still maintained compared with bare-Al and patterned-Al electrodes. These results are in good agreement with Figures 6 and S9.

Therefore, in this study, improved ultrafast (at current density of 20 C) and ultra-stable (during the 1000 cycles) cycling performances of the NF-G@patterned-Al electrode

have been achieved by forming the novel micropatterns with N- and F-doped graphene interfacial layer on Al foil. The improvement factor of cycling performances can be attributed to the two major effects of the N- and F-doped graphene interfacial layer of micropatterned Al foil (Figure 8): (I) the micro-patterns on Al foil can increase the collection/provision site of electrons with a high contact area between the electrode and the current collector, enhancing the ultrafast cycling capacity; (II) the applied N- and F-doped graphene interfacial layer effectively prevents the corrosion of the current collector by graphene as a conductive passivation layer and provides a fast charge transfer on the interface by doped N and F atoms, leading to superb ultrafast cycling stability.

CONCLUSIONS

Here, we successfully fabricated an N- and F-doped graphene interfacial layer on micropatterned Al foil as the current collector using roll pressing and dip coating processes. Specifically, we proposed a unique interface morphology of micropatterns and the N- and F-doped graphene interfacial layer on Al foil, which can offer improved ultrafast and ultra-stable cycling performances. The NF-G@patterned-Al indicated the micropattern size in the range from ~ 326.8 – 348.8 μm (aspect ratio of 3.09) and the N- and F-doped graphene layer with a thickness of ~ 0.48 – 0.61 μm . In addition, this structure exhibited the improved effects of Li ion diffusion efficiency (1.80×10^{-12} $\text{cm}^2 \text{s}^{-1}$). When the NF-G@patterned-Al was applied as the current collector at the electrode for the LIBs, an ultrafast and ultra-stable cycling performance of 87.1 mA h g^{-1} with a capacity retention of 82.3% after 1000 cycles at 20 C and an excellent cycling stability of 168.8 mA h g^{-1} with a capacity retention of 84.1% after 500 cycles at 1 C were clearly observed. This can be ascribed to the following efficient functionalities of the micropatterns with the N- and F-doped graphene interfacial layer on Al foil. First, superb ultrafast cycling capacity is caused by the increased collection/provision site of electrons with a high contact area between the electrode and the current collector resulting from the formation of micropatterns on Al foil. Second, improved ultrafast cycling stability is related to the prevented corrosion of Al foil by fast charge transfer of the N- and F-doped graphene interface as a conductive passivation layer. Therefore, the N- and F-doped graphene interfacial layer on micropatterned Al foil is a promising strategy for improving the ultrafast and ultra-stable lithium storage performance in LIBs.

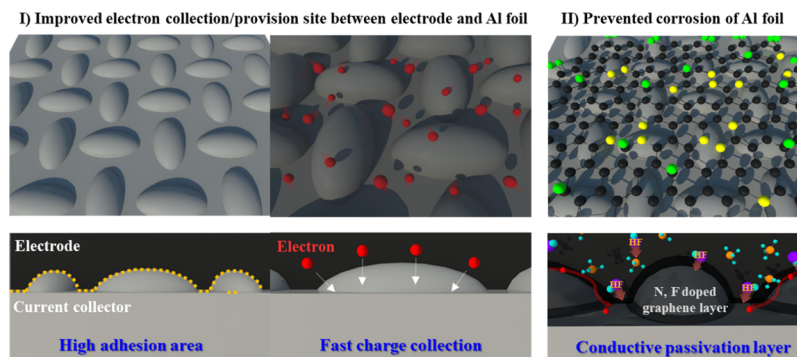


Figure 8. Schematic illustration of the two main effects on the NF-G@patterned-Al electrode for enhancing ultrafast and ultra-stable cycling performances. (I) Effect of micropatterns on Al foil and (II) effect of the N and F doped graphene interfacial layer on micropatterned Al foil.

EXPERIMENTAL SECTION

Brief description of experimental methods is explained in Figure 1. Details of processes and synthesis conditions used in this study are provided in Supporting Information.

ASSOCIATED CONTENT

Supporting Information

The Supporting Information is available free of charge at <https://pubs.acs.org/doi/10.1021/acsami.0c01774>.

Experimental sections, additional SEM and OM images of micropatterns and graphene, TGA data of precursor used to N- and F-doped graphene, LSM images of samples, Raman spectroscopy obtained from graphene and N- and F-doped graphene, charge–discharge curves of electrodes and schematic illustration of doping and reaction mechanism of samples, and EDS mapping images of samples (PDF)

AUTHOR INFORMATION

Corresponding Author

Hyo-Jin Ahn – Program of Materials Science & Engineering, Convergence Institute of Biomedical Engineering and Biomaterials and Department of Materials Science and Engineering, Seoul National University of Science and Technology, Seoul 01811, Korea; orcid.org/0000-0002-5786-3937; Email: hjahn@seoultech.ac.kr

Author

Dong-Yo Shin – Program of Materials Science & Engineering, Convergence Institute of Biomedical Engineering and Biomaterials, Seoul National University of Science and Technology, Seoul 01811, Korea

Complete contact information is available at: <https://pubs.acs.org/doi/10.1021/acsami.0c01774>

Notes

The authors declare no competing financial interest.

ACKNOWLEDGMENTS

This work was supported by the National Research Foundation of Korea (NRF) grant funded by the Korea government (MSIT) (no. 2019R1 A2 C1005836).

REFERENCES

- (1) Pmnerantseva, E.; Bonaccorso, F.; Feng, X.; Cui, Y.; Gogotsi, Y. Energy storage: the future enabled by nanomaterials. *Science* **2019**, *366*, No. eaan8285.
- (2) Maurel, A.; Grugeon, S.; Fleutot, B.; Courty, M.; Prashantha, K.; Tortajada, H.; Armand, M.; Panier, S.; Dupont, L. Three-dimensional printing of a LiFePO₄/graphite battery cell via fused deposition modeling. *Sci. Rep.* **2019**, *9*, 18031.
- (3) Zhang, M.; Xiang, L.; Galluzzi, M.; Jiang, C.; Zhang, S.; Li, J.; Tang, Y. Uniform Distribution of Alloying/Dealloying Stress for High Structural Stability of an Al Anode in High-Areal-Density Lithium-Ion Batteries. *Adv. Mater.* **2019**, *31*, 1900826.
- (4) Shin, D.-Y.; Sung, K.-W.; Ahn, H.-J. Synergistic effect of heteroatom-doped activated carbon for ultrafast charge storage kinetics. *Appl. Surf. Sci.* **2019**, *478*, 499.
- (5) An, G.-H.; Lee, D.-Y.; Ahn, H.-J. Tunneled mesoporous carbon nanofibers with embedded ZnO nanoparticles for ultrafast lithium storage. *ACS Appl. Mater. Interfaces* **2017**, *9*, 12478.
- (6) Qin, P.; Wang, M.; Li, N.; Zhu, H.; Ding, X.; Tang, Y. Bubble-Sheet-Like Interface Design with an Ultrastable Solid Electrolyte Layer for High-Performance Dual-Ion Batteries. *Adv. Mater.* **2017**, *29*, 1606805.
- (7) Zhou, X.; Liu, Q.; Jiang, C.; Ji, B.; Ji, X.; Tang, Y.; Cheng, H. M. Strategies towards Low-Cost Dual-Ion Batteries with High Performance. *Angew. Chem., Int. Ed.* **2020**, *59*, 3802.
- (8) Sin, D.-Y.; Koo, B.-R.; Ahn, H.-J. Hollow lithium manganese oxide nanotubes using MnO₂-carbon nanofiber composites as cathode materials for hybrid capacitors. *J. Alloys Compd.* **2017**, *696*, 290.
- (9) Zhu, G.; Wang, L.; Lin, H.; Ma, L.; Zhao, P.; Hu, Y.; Chen, T.; Chen, R.; Wang, Y.; Tie, Z.; Liu, J.; Jin, Z. Walnut-like multicore-shell MnO encapsulated nitrogen-rich carbon nanocapsules as anode material for long-cycling and soft-packed lithium-ion batteries. *Adv. Funct. Mater.* **2018**, *28*, 1800003.
- (10) Yang, H.; Wu, H. H.; Ge, M.; Li, L.; Yuan, Y.; Yao, Q.; Chen, J.; Xia, L.; Zheng, J.; Chen, Z.; Duan, J.; Kisslinger, K.; Zeng, X. C.; Lee, W. K.; Zhang, Q.; Lu, J. Simultaneously dual modification of Ni-rich layered oxide cathode for high-energy lithium-ion batteries. *Adv. Funct. Mater.* **2019**, *29*, 1808825.
- (11) An, G.-H.; Lee, D.-Y.; Lee, Y.-J.; Ahn, H.-J. Ultrafast lithium storage using antimony-doped tin oxide nanoparticles sandwiched between carbon nanofibers and a carbon skin. *ACS Appl. Mater. Interfaces* **2016**, *8*, 30264.
- (12) Shin, D.-Y.; Park, D.-H.; Ahn, H.-J. Interface modification of an Al current collector for ultrafast lithium-ion batteries. *Appl. Surf. Sci.* **2019**, *475*, 519.
- (13) Ma, T.; Xu, G.-L.; Li, Y.; Wang, L.; He, X.; Zheng, J.; Liu, J.; Engelhard, M. H.; Zapol, P.; Curtiss, L. A.; Jorne, J.; Amine, K.; Chen, Z. Revisiting the corrosion of the aluminum current collector in lithium-ion batteries. *J. Phys. Chem. Lett.* **2017**, *8*, 1072.
- (14) Wang, M.; Tang, M.; Chen, S.; Ci, H.; Wang, K.; Shi, L.; Lin, L.; Ren, H.; Shan, J.; Gao, P.; Liu, Z.; Peng, H. Graphene-armored aluminum foil with enhanced anticorrosion performance as current collectors for lithium-ion batteries. *Adv. Mater.* **2017**, *29*, 1703882.
- (15) Lepage, D.; Savignac, L.; Saulnier, M.; Gervais, S.; Schougaard, S. B. Modification of aluminum current collectors with a conductive polymer for application in lithium batteries. *Electrochem. Commun.* **2019**, *102*, 1.
- (16) Teucher, G.; Van Gestel, T.; Krott, M.; Gehrke, H.-G.; Eichel, R.-A.; Uhlenbruck, S. Processing of Al-doped ZnO protective thin films on aluminum current collectors for lithium ion batteries. *Thin Solid Films* **2016**, *619*, 302.
- (17) Huang, S.; Li, Y.; Feng, Y.; An, H.; Long, P.; Qin, C.; Feng, W. Nitrogen and fluorine co-doped graphene as a high-performance anode material for lithium-ion batteries. *J. Mater. Chem. A* **2015**, *3*, 23095.
- (18) Chun, J.; Jo, C.; Sahgong, S.; Kim, M. G.; Lim, E.; Kim, D. H.; Hwang, J.; Kang, E.; Ryu, K. A.; Jung, Y. S.; Kim, Y.; Lee, J. Ammonium fluoride mediated synthesis of anhydrous metal fluoride-mesoporous carbon nanocomposites for high-performance lithium ion battery cathodes. *ACS Appl. Mater. Interfaces* **2016**, *8*, 35180.
- (19) An, Y.; Fei, H.; Zeng, G.; Xu, X.; Ci, L.; Xi, B.; Xiong, S.; Feng, J.; Qian, Y. Vacuum distillation derived 3D porous current collector for stable lithium-metal batteries. *Nano Energy* **2018**, *47*, 503.
- (20) Hsieh, Y.-Y.; Fang, Y.; Daum, J.; Kanakaraj, S. N.; Zhang, G.; Mishra, S.; Gbordzoe, S.; Shanov, V. Bio-inspired, nitrogen doped CNT-graphene hybrid with amphiphilic properties as a porous current collector for lithium-ion batteries. *Carbon* **2019**, *145*, 677.
- (21) Lu, H.; Hagberg, J.; Lindbergh, G.; Cornell, A. Li₄Ti₅O₁₂ flexible, lightweight electrodes based on cellulose nanofibrils as binder and carbon fibers as current collectors for Li-ion batteries. *Nano Energy* **2017**, *39*, 140.
- (22) Richard Prabakar, S. J.; Hwang, Y.-H.; Bae, E. G.; Lee, D. K.; Pyo, M. Graphene oxide as a corrosion inhibitor for the aluminum current collector in lithium ion batteries. *Carbon* **2013**, *52*, 128.
- (23) Monteserín, C.; Blanco, M.; Aranzabe, E.; Aranzabe, A.; Laza, J. M.; Larrañaga-Varga, A.; Vilas, J. L. Effects of graphene oxide and chemically-reduced graphene oxide on the dynamic mechanical properties of epoxy amine composites. *Polymers* **2017**, *9*, 449.

(24) Zhang, W.; Fu, Y.; Liu, W.; Lim, L.; Wang, X.; Yu, A. A general approach for fabricating 3D MFe_2O_4 (M=Mn, Ni, Cu, Co)/graphitic carbon nitride covalently functionalized nitrogen-doped graphene nanocomposites as advanced anodes for lithium-ion batteries. *Nano Energy* **2019**, *57*, 48.

(25) Gupta, B.; Kumar, N.; Panda, K.; Kanan, V.; Joshi, S.; Visoly-fisher, I. Role of oxygen functional groups in reduced graphene oxide for lubrication. *Sci. Rep.* **2017**, *7*, 45030.

(26) Kim, J.; Zhou, R.; Murakoshi, K.; Yasuda, S. Advantage of semi-ionic bonding in fluorine-doped carbon materials for the oxygen evolution reaction in alkaline media. *RSC Adv.* **2018**, *8*, 14152.

(27) Usachov, D. Y.; Bokai, K. A.; Marchenko, D. E.; Fedorov, A. V.; Shevelev, V. O.; Vilkov, O. Y.; Kataev, E. Y.; Yashina, L. V.; Rühl, E.; Laubschat, C.; Vyalikh, D. V. Cobalt-assisted recrystallization and alignment of pure and doped graphene. *Nanoscale* **2018**, *10*, 12123.

(28) An, H.; Li, Y.; Gao, Y.; Cao, C.; Han, J.; Feng, Y.; Feng, W. Free-standing fluorine and nitrogen co-doped graphene paper as a high-performance electrode for flexible sodium-ion batteries. *Carbon* **2017**, *116*, 338.

(29) Yuan, D.; Wei, Z.; Han, P.; Yang, C.; Huang, L.; Gu, Z.; Ding, Y.; Ma, J.; Zheng, G. Electron distribution tuning of fluorine-doped carbon for ammonia electrosynthesis. *J. Mater. Chem. A* **2019**, *7*, 16979.

(30) Wang, Q.; Ji, Y.; Lei, Y.; Wang, Y.; Wang, Y.; Li, Y.; Wang, S. Pyridinic-N-dominated doped defective graphene as a superior oxygen electrocatalyst for ultrahigh-energy-density Zn-air batteries. *ACS Energy Lett.* **2018**, *3*, 1183.

(31) Wang, Q.; Lei, Y.; Zhu, Y.; Wang, H.; Feng, J.; Ma, G.; Wang, Y.; Li, Y.; Nan, B.; Feng, Q.; Lu, Z.; Yu, H. Edge defect engineering of nitrogen-doped carbon for oxygen electrocatalysts in Zn-air batteries. *ACS Appl. Mater. Interfaces* **2018**, *10*, 29448.

(32) Mao, J.; Iocozzia, J.; Huang, J.; Meng, K.; Lai, Y.; Lin, Z. Graphene aerogels for efficient energy storage conversion. *Energy Environ. Sci.* **2018**, *11*, 772.

(33) Andre, D.; Meiler, M.; Steiner, K.; Wimmer, C.; Soczka-Guth, T.; Sauer, D. U. Characterization of high-power lithium-ion batteries by electrochemical impedance spectroscopy. I. experimental investigation. *J. Power Sources* **2011**, *196*, 5334.

(34) Nara, H.; Mukoyama, D.; Shimizu, R.; Momma, T.; Osaka, T. Systematic analysis of interfacial resistance between the cathode layer and the current collector in lithium-ion batteries by electrochemical impedance spectroscopy. *J. Power Sources* **2019**, *409*, 139.

(35) Wu, Z.; Qiu, W.; Chen, Y.; Luo, Y.; Huang, Y.; Lei, Q.; Guo, S.; Liu, P.; Balogun, M.-S.; Tong, Y. Etched current collector-guided creation of wrinkles in steel-mesh-supported V_6O_{13} cathode for lithium-ion batteries. *J. Mater. Chem. A* **2017**, *5*, 756.

(36) An, G.-H.; Kim, H.; Ahn, H.-J. Improved ionic diffusion through the mesoporous carbon skin on silicon nanoparticles embedded in carbon for ultrafast lithium storage. *ACS Appl. Mater. Interfaces* **2018**, *10*, 6235.